

AperTO - Archivio Istituzionale Open Access dell'Università di Torino

Superoxide-driven autocatalytic dark production of hydroxyl radicals in the presence of complexes of natural dissolved organic matter and iron

This is the author's manuscript

Original Citation:

Availability:

This version is available <http://hdl.handle.net/2318/1932291> since 2024-11-25T09:05:17Z

Published version:

DOI:10.1016/j.watres.2020.115782

Terms of use:

Open Access

Anyone can freely access the full text of works made available as "Open Access". Works made available under a Creative Commons license can be used according to the terms and conditions of said license. Use of all other works requires consent of the right holder (author or publisher) if not exempted from copyright protection by the applicable law.

(Article begins on next page)

1 Superoxide-driven autocatalytic dark production of
2 hydroxyl radicals in the presence of complexes of
3 natural dissolved organic matter and iron

4 *Yihua Xiao*^{1*}, *Luca Carena*², *Marja-Terttu Näsi*¹, *Anssi V. Vähätalo*¹

5 ¹Department of Biological and Environmental Science, University of Jyväskylä, 40014
6 Jyväskylä, Finland

7 ²Dipartimento di Chimica, Università di Torino, Via Pietro Giuria 5, 10125 Torino, Italy

8

9 *Corresponding author: yihua.y.xiao@jyu.fi

10

11

12 **Abstract**

13 We introduced superoxide as potassium superoxide (KO_2) to artificial lake water containing
14 dissolved organic matter (DOM) without or with introduced ferric iron complexes (DOM-Fe),
15 and monitored the production rate of hydroxyl radicals as well as changes in the absorption and
16 fluorescence properties of DOM. The introduction of KO_2 decreased the absorption by DOM
17 but increased the spectral slope coefficient of DOM more with complexed ferric Fe than
18 without it. The introduction of KO_2 increased the fluorescence of humic-like components in
19 DOM without introduced ferric Fe but resulted in the loss of fluorescence in DOM with
20 introduced ferric Fe. A single introduction of $13 \mu\text{mol L}^{-1} \text{KO}_2$ produced $10 \mu\text{mol L}^{-1}$ and 104
21 $\mu\text{mol L}^{-1}$ hydroxyl radicals during a week-long experiment without and with the introduced
22 DOM-Fe complexes, respectively. The production rate of hydroxyl radicals decreased
23 exponentially with time but levelled off and continued several days in DOM with introduced
24 ferric Fe. These findings suggest that in the presence of DOM-Fe complexes, superoxide can
25 trigger an autocatalytic Fenton reaction that produces hydroxyl radicals and breaks down DOM.

26 **Keywords:** dissolved organic matter, iron, superoxide, hydroxyl radicals, production rate,
27 absorption

28

29 **1 Introduction**

30 Dissolved organic matter (DOM) is a heterogeneous mixture of organic compounds and
31 plays important roles in natural and engineered systems. In soils and freshwaters, the majority
32 of DOM consists of humic substances that primarily originate from terrestrial plant litter after
33 biotic and abiotic transformations (Piccolo, 1996; Tranvik, 1988). Humic DOM binds ferric
34 iron, Fe(III), into complexes, DOM-Fe(III), and keeps poorly soluble Fe(III) in dissolved form
35 (Fujii et al., 2014). Humic DOM contains aromatic and quinone-like moieties, which occur in
36 three redox-states (quinones, semiquinones and hydroquinones) and can mediate reactions
37 between electron donors and acceptors with Fe (Aeschbacher et al., 2010; Chen & Pignatello,
38 1997; Garg et al., 2018; Yuan et al., 2016).

39 The enzymatic hydrolysis of humic DOM and its intracellular metabolism is inefficient,
40 because the large size of molecular aggregates, chemical heterogeneity, and non-hydrolysable
41 bonds limit the microbial transformation of humic DOM (Arnosti, 2004). Abiotic
42 photochemical reactions mineralize humic DOM and account for one tenth of CO₂ emissions
43 in freshwaters (Aarnos et al., 2018; Koehler et al., 2014). The remaining 90% of DOM is
44 mineralized through mechanisms that are poorly known.

45 Extracellular reactions between DOM and reactive oxygen species (ROS) can explain
46 a part of DOM transformations (Mostovaya et al., 2017; Page et al., 2012; Trusiak et al., 2018;
47 Waggoner et al., 2017). The first step in the formation of ROS is a one-electron reduction of
48 O₂ to superoxide (O₂^{•-}). Numerous processes produce O₂^{•-}: (i) photochemical reactions
49 (Micinski et al., 1993; Fujii & Otani, 2017; Zhang & Blough, 2016; Text SIV in supporting
50 information (SI)), (ii) abiotic dark oxidation of reduced metals or organic matter (Garg et al.,
51 2018; Gil-Lozano et al., 2017; Page et al., 2012; Yuan et al., 2016) and (iii) biological processes
52 both in light and dark (Diaz et al., 2013; Diaz & Plummer, 2018; Imlay, 2004; Zhang et al.,
53 2016). O₂^{•-} reacts with the redox-active metals (e.g., Fe and copper) and quinone-like moieties

54 of DOM, but it has otherwise limited reactivity with aqueous DOM (Garg et al., 2011, 2018;
55 Hayyan et al., 2016; Yuan et al., 2016).

56 $O_2^{\bullet-}$ can be reduced further to hydrogen peroxide (H_2O_2) and hydroxyl radicals ($\bullet OH$).
57 Bimolecular disproportionation and the disproportionation catalyzed by reduced metals or
58 DOM transform $O_2^{\bullet-}$ to H_2O_2 (Goldstone & Voelker, 2000; Ma et al., 2010). $O_2^{\bullet-}$ can reduce
59 DOM-Fe(III) to DOM-Fe(II) (Rose & Waite, 2005). DOM-Fe(II) as well as inorganic Fe(II)
60 can react with H_2O_2 through the Fenton reaction and produce highly reactive $\bullet OH$ that breaks
61 down DOM (Southworth & Voelker, 2003; Voelker et al., 1997).



63 According to the stoichiometry of the Fenton reaction (Eq. 1), the Fe(III)-catalyzed
64 production of $\bullet OH$ requires three $O_2^{\bullet-}$ radicals, two for the formation of H_2O_2 and one for the
65 formation of DOM-Fe(II). However, the stoichiometry of the Fenton reaction ($\bullet OH$ -to- $O_2^{\bullet-}$
66 ratio = 0.33) ignores a well-known fact that $\bullet OH$ generates radical species that can regenerate
67 the Fenton reactants and autocatalyze the Fenton reaction (e.g., Chen & Pignatello, 1997; Gil-
68 Lozano et al., 2017). The degree of autocatalysis is poorly known, although it has high
69 importance when the efficiency of the Fenton reaction is evaluated in natural or engineered
70 systems.

71 The present study estimates the dark production rates of $\bullet OH$ in artificial lake water
72 from $O_2^{\bullet-}$ (introduced as potassium superoxide, KO_2) in the presence of DOM with or without
73 introduced Fe(III). The production rates of $\bullet OH$ were quantified from the reaction between
74 $\bullet OH$ and coumarin (Louit et al., 2005) and after accounting for the major scavengers of $\bullet OH$
75 in the artificial lake water. In this study we demonstrate that the cumulative production of $\bullet OH$
76 from $O_2^{\bullet-}$ in a-week-long experiment exceeds the $\bullet OH$ yield of the Fenton reaction by several
77 folds and extensively modifies the spectroscopic properties of DOM.

78

79 2 Materials and methods

80 2.1 Materials and reagents

81 DOM was extracted from a water sample collected during the fall turnover of Lake
82 Valkea-Kotinen in southern Finland. This small headwater lake is acidic (pH 5.4) with high
83 concentration of DOC ($10\text{--}12\text{ mg DOC L}^{-1} = \sim 20\text{ mg DOM L}^{-1}$) and total Fe ($\sim 5\text{ }\mu\text{M}$; Einola
84 et al., 2011; Vähätalo et al., 2003). In Lake Valkea-Kotinen, the mean molecular mass of DOM
85 is $1130\text{--}4000\text{ g mol}^{-1}$, the content of humic substances and aromatic groups is 75% and
86 45–67%, respectively (Vogt et al., 2004).

87 The extraction of DOM followed the method by Dittmar et al. (2008) but included an
88 addition of 0.01 M sodium fluoride (NaF, Sigma-Aldrich) in filtered ($<0.2\text{ }\mu\text{m}$) and acidified
89 (pH 2) lake water. At pH 2, Fe(III) binds poorly on DOM and preferentially forms ferric
90 fluoride complex (Gao & Zepp, 1998). Ferric fluoride and fluoride ions were rinsed out of the
91 column with 0.01 M HCl (Dittmar et al. 2008) to yield extracted DOM with a very low content
92 of fluoride and Fe. The extraction removed 96.6% of Fe from lake water and the DOM extracts
93 contained 8.5 nmol Fe/mg DOM (Table 1). The chemicals ($>97\%$ pure) were bought from
94 Sigma Aldrich. Iron(III) chloride hexahydrate ($\text{FeCl}_3\cdot 6\text{H}_2\text{O}$) and KO_2 were the sources of
95 Fe(III) and $\text{O}_2^{\bullet-}$, respectively. Coumarin and 7OH-coumarin were the probes for $\bullet\text{OH}$ (Burgos
96 Castillo et al., 2018). The aqueous solutions were prepared in ultrapure water (resistivity 18
97 $\text{M}\Omega\cdot\text{cm}$; SG ultrapure water system, SG WATER), but were later modified to artificial lake
98 water by a salt solution mixture (Table S1). Glassware was soaked overnight in 0.1 M HCl and
99 carefully rinsed with ultrapure water six times prior to use.

100 2.2 Experimental setup

101 The experiment consisted of four treatments prepared in triplicates (Table 1):

- 102 1) “control” – extracted DOM (8.5 nmol Fe/mg DOM) dissolved in artificial lake water;
- 103 2) “ KO_2 ” – like (1) but with introduced KO_2 ;

104 3) “Fe” – like (1) but Fe(III) was introduced as DOM-Fe(III) (1000 nmol Fe(III)/mg
105 DOM);

106 4) “Fe + KO₂” – a combination of (2) and (3).

107 For the preparation of DOM-Fe(III), the acidic (pH 2) DOM solution (50 mg L⁻¹ in
108 ultrapure water) received 1 mM Fe(III) and was titrated to pH 5 with NaOH and HCl,
109 approximating the ambient pH of Lake Valkea-Kotinen. During the titration, the binding sites
110 of DOM suppressed the hydrolysis of ferric Fe and DOM-Fe(III) was formed (Karlsson &
111 Persson, 2012). According to an equilibrium speciation model (Visual Minteq 3.1), the DOM
112 extract was able to bind Fe(III) entirely and accordingly visual precipitates were absent at any
113 phase of the experiment. The “control” and “KO₂” treatments were titrated in the same way
114 but without the introduced Fe. All treatments received the stock solution of coumarin to the
115 final concentration of 10 μM (Table 1) and inorganic component of artificial lake water (Table
116 S1).

117 The “KO₂” and “Fe + KO₂” treatments received an alkaline solution of KO₂ (2 g KO₂
118 in 100 mL 0.05 M NaOH) to a 13 μM final concentration (Table 1). Similar magnitudes of
119 O₂^{•-} form instantly during the oxidation of reduced organic matter or metals (Liao et al., 2019;
120 Minella et al., 2015; Page et al., 2013; Trusiak et al., 2018; Zhang & Yuan, 2017), with a few
121 days of microbial metabolism (Zhang et al., 2016) or with 0.17–few days of solar irradiation
122 depending on water quality (Cooper & Zika, 1983; Micinski et al., 1993; Text SIV in SI). The
123 introduction of KO₂ increased the pH of non-buffered artificial lake water to 12.2, where the
124 reduction rate of DOM-Fe(III) to DOM-Fe(II) by O₂^{•-} is faster than bimolecular
125 disproportionation of O₂^{•-} (see Text SI in SI). The reaction medium was titrated back to pH 5
126 with HCl. Finally, all treatments were incubated at 20 °C in the dark with a headspace of air.

127 2.3 UV-Vis spectral analysis

128 After 26 h and a week (168 h) of incubation, the absorbance of chromophoric DOM

129 (CDOM) was measured with a UV-Vis spectrometer (Lambda 850, PerkinElmer) from 200 nm
130 to 700 nm at 1 nm intervals. The absorption coefficient was calculated as,

$$131 \quad a_{\lambda} = 2.303 \times A_{\lambda}/L \quad \text{Eq. 2,}$$

132 where a_{λ} (m^{-1}) is the absorption coefficient at wavelength λ , A_{λ} (unitless) is absorbance, and L
133 is the path length of the cuvette ($L = 0.01$ m). The changes in a_{λ} were quantified at 410 nm as
134 a_{410} , an indicator of water color (Hongve et al., 2004). The spectral slope coefficient ($S_{275-295}$),
135 which indicates the molecular mass of DOM, was calculated from ln-transformed absorption
136 coefficient between 275 nm and 295 nm (Helms et al., 2008).

137 2.4 Fluorescence analysis and PARAFAC

138 Samples for fluorescence analysis were stored at 4 °C after collection and measured
139 within 3 weeks. Fluorescence EEMs were measured with a LS 55 luminescence spectrometer
140 (PerkinElmer). The samples were scanned with an excitation wavelength (Ex) from 240 nm to
141 450 nm at 5 nm intervals and emission wavelength (Em) from 300 nm to 600 nm with 0.5 nm
142 intervals. The slit width for both Ex and Em was set to 5 nm. Blank and Raman samples from
143 ultrapure water were measured prior to actual samples (Murphy et al., 2003).

144 PARALLEL FACTOR analysis (PARAFAC) was run in Matlab R2015b (Mathworks, USA)
145 using the drEEM toolbox (version 0.3.0). The raw EEM dataset ($n = 48$) was corrected for
146 spectral bias, inner filter effects and background signals (measured with ultrapure water). In
147 the end, all EEMs were normalized to the area of Raman peak collected with ultrapure water
148 at Ex = 275 nm to compensate for daily fluctuations in lamp intensity (Kothawala et al., 2016;
149 Murphy et al., 2013). The fluorescent components were validated with multiple split-half tests.
150 The validation was constrained by a Tucker congruence coefficient (TCC >0.95). Finally, the
151 maximum fluorescence intensities (F_{max} , in Raman unit, R.U.) of components were reported.

152 2.5 Calculations of the cumulative production of •OH radicals

153 The samples for the quantification of coumarin and 7OH-coumarin were collected at 0,

154 3, 6, 20, 26, and 168 h. These samples were frozen immediately after collection and analyzed
155 later. Coumarin and 7OH-coumarin were measured by high performance liquid
156 chromatography (HPLC) equipped with UV-Vis absorbance and fluorescence detectors (Louit
157 et al., 2005). The quantification of the two compounds was carried out by means of the UV-
158 Vis absorbance detector for coumarin (absorption wavelength = 280 nm) and fluorescence
159 detector for 7OH-coumarin (excitation wavelength = 320 nm; emission wavelength = 450 nm).
160 The Text SII in SI reports the details of HPLC technique.

161 The formation rates of $\bullet\text{OH}$ were quantified from the reaction between coumarin and
162 $\bullet\text{OH}$. This reaction has a second-order rate constant of $5.6 \times 10^9 \text{ M}^{-1} \text{ s}^{-1}$ and produces a few
163 hydroxycoumarin isomers, including 7OH-coumarin with a yield of 0.047 (Burgos Castillo et
164 al., 2018). We calculated the production rates of $\bullet\text{OH}$ along the course of the experiment by
165 quantifying periodically the concentrations of 7OH-coumarin and coumarin as well as
166 accounting for the scavenging of $\bullet\text{OH}$ by DOM, Cl^- , HCO_3^- , coumarin and 7OH-coumarin.
167 The calculations assumed a steady-state between the scavenging and the formation rate of $\bullet\text{OH}$.
168 The production rates of $\bullet\text{OH}$ radicals were integrated over the course of the experiment for the
169 cumulative production of $\bullet\text{OH}$. The detailed procedure for calculations is described in the SI.

170 2.6 Statistical analyses

171 The statistical difference between the triplicated treatments and control (DOM alone
172 treatment) was assessed using paired t tests with two-tailed distributions. The significance level
173 was set at $P < 0.05$.

174 **3 Results**

175 3.1 Changes in absorption spectra

176 The introduction of KO_2 did not change the absorption coefficient a_{410} in an early phase
177 of the experiment (at 26 h) but decreased it by 25% by the end of the experiment (at 168 h)
178 compared to DOM in artificial lake water without KO_2 (“control” vs “ KO_2 ”, Figure 1a). In the

179 “Fe” treatment, the introduced DOM-Fe(III) consistently kept a_{410} at a higher level than in the
180 control (Figure 1a). When introduced with DOM-Fe(III), KO_2 decreased a_{410} by 18% already
181 at 26 h and by 66% over the entire experiment compared to the control (“Fe + KO_2 ”, Figure
182 1a).

183 In comparison with the control treatment, KO_2 increased the spectral slope coefficient
184 ($S_{275-295}$), while DOM-Fe(III) decreased it (Figure 1b). When introduced with Fe, KO_2
185 increased $S_{275-295}$ by 20% at 26 h and by 54% at the end of the experiment (Figure 1b).

186 3.2 Changes in fluorescent intensities of PARAFAC components

187 The four components of fluorescent DOM identified by the EEM-PARAFAC
188 associated with humic substances (Comp 1–2, Figure 2 and Table S2), 7OH-coumarin (Comp
189 3; Figure S1) and protein-like DOM (Comp 4, Figure 2 and Table S2). After 168 h, the
190 introduction of KO_2 had increased the fluorescence of humic-like components 1 and 2 by 39%
191 and 18%, respectively, in comparison to the control treatment (“ KO_2 ”, Figure 3). The added
192 associated Fe(III) quenched the fluorescence of humic-like components 1–2 (“Fe”, Figure 3).
193 In the presence of DOM-Fe(III), KO_2 reduced the fluorescence of components 1–2 relative to
194 the control treatment and decreased the fluorescence of component 4 to negligible level (“Fe +
195 KO_2 ”, Figure 3). Component 3 was detected in all treatments (Figure 3) indicating that $\bullet OH$
196 radicals transformed coumarin (Table 1) into 7OH-coumarin, as explained in the following
197 section.

198 3.3 Production of $\bullet OH$

199 The formation rate of $\bullet OH$, $R_f^{\bullet OH}(t)$, was assessed from the measured concentrations
200 of coumarin and 7OH-coumarin (Figure SIII-1&2) accounting for the other scavengers of $\bullet OH$
201 as described in the Text SIII in SI. In the beginning of the experiment, $R_f^{\bullet OH}(t_0)$ was
202 0.0031–0.0034 $nM s^{-1}$ in the “Fe” treatment and the control, which did not receive KO_2 (Figure

203 4; Table SIII-1). The introduction of KO_2 resulted in $R_f^{\bullet\text{OH}}(t_0)$ of 0.039 nM s^{-1} and 1.14 nM s^{-1}
204 ¹ in the “ KO_2 ” and “ $\text{KO}_2 + \text{Fe}$ ”-treatments, respectively (Figure 4; Table SIII-1). In the “ KO_2
205 $+ \text{Fe}$ ” treatment, the measured $R_f^{\bullet\text{OH}}(t_0)$ was nearly identical to the corresponding rate of 1.05
206 nM s^{-1} calculated based on a simple kinetic model (Figure SI-2). Briefly, the calculated rates
207 are based on the kinetics for the following sequence of reactions: (i) the reduction of DOM-
208 Fe(III) to $13 \text{ }\mu\text{M}$ DOM- Fe(II) by $\text{O}_2^{\bullet-}$, (ii) the reduction of O_2 to $\text{O}_2^{\bullet-}$ by DOM- Fe(II) , (iii) the
209 disproportionation of $\text{O}_2^{\bullet-}$ to H_2O_2 and (iv) the Fenton reaction (Eq. 1) between H_2O_2 and
210 DOM- Fe(II) . The good match between the measured and the calculated $R_f^{\bullet\text{OH}}(t_0)$ in the “ KO_2
211 $+ \text{Fe}$ ” treatment suggest that, (i) $\text{O}_2^{\bullet-}$ induced the formation of $\bullet\text{OH}$ in the presence of DOM-
212 Fe(III) and (ii) the reaction stoichiometry (e.g., $\bullet\text{OH}$ -to- $\text{O}_2^{\bullet-}$ ratio = 0.33 of Eq. 1) described
213 the measured initial rates well.

214 The formation rates of $\bullet\text{OH}$ decreased exponentially with time in all treatments, and
215 after 10 h levelled at 0.15 nM s^{-1} in the “ $\text{KO}_2 + \text{Fe}$ ” treatment (Figure 4, Table SIII-1). In the
216 “ $\text{KO}_2 + \text{Fe}$ ” treatment, the prolonged formation of $\bullet\text{OH}$ is consistent with the changes in DOM
217 that took place mostly after 26 h (Figure 1), but inconsistent with a simple kinetic model (Text
218 SI-3). The simple kinetic model incorrectly suggests the depletion of $R_f^{\bullet\text{OH}}(t)$ within a few
219 minutes (Text SI-3) in contrast to the measured $R_f^{\bullet\text{OH}}(t)$, which lasted tens of hours (Figure 4).

220 The cumulative production of $\bullet\text{OH}$ was computed as the integral of $R_f^{\bullet\text{OH}}(t)$ for the first
221 10 hours or for the entire length of the experiment (168 h, Table 2, Eq. SIII-1). In all treatments,
222 the majority of $\bullet\text{OH}$ was produced after 10 h (Table 2). In the treatments with introduced KO_2 ,
223 the cumulative production of $\bullet\text{OH}$ was 9.9 and $104 \text{ }\mu\text{M}$ in the “ KO_2 ” and “ $\text{KO}_2 + \text{Fe}$ ” treatments,
224 respectively, over the entire length of the experiment (Table 2). The yields of $\bullet\text{OH}$ per
225 introduced $13 \text{ }\mu\text{M}$ KO_2 were $0.76 \bullet\text{OH}/\text{O}_2^{\bullet-}$ and $8 \bullet\text{OH}/\text{O}_2^{\bullet-}$ in the “ KO_2 ” and “ $\text{KO}_2 + \text{Fe}$ ”
226 treatments, respectively. The measured yields exceeded the stoichiometric yield (0.33

227 $\bullet\text{OH}/\text{O}_2\bullet^-$ in Eq. 1) by a factor of 2.3 and 24 in the “ KO_2 ” and “ $\text{KO}_2 + \text{Fe}$ ” treatments,
228 respectively, and indicated an autocatalytic formation of $\bullet\text{OH}$ from $\text{O}_2\bullet^-$ in the presence of
229 DOM-Fe.

230

231 **4 Discussion**

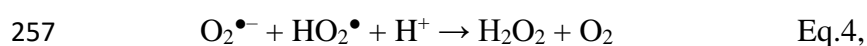
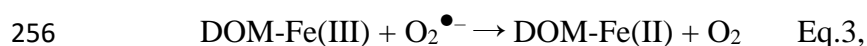
232 4.1 $\bullet\text{OH}$ production

233 As explained in the Method-section 2.2, the amount of introduced $\text{O}_2\bullet^-$ in this study is
234 environmentally relevant but here we compare the cumulative productions of $\bullet\text{OH}$ (0.23–104
235 μM) in our week-long experiment to those reported earlier. An oxidation of reduced DOM or
236 metals produces $\bullet\text{OH}$. For example, the oxidation of Arctic surface and soil waters produce
237 0.2–4.5 μM $\bullet\text{OH}$ over 24 hour oxidation (Page et al., 2013); the oxidation of hypolimnetic
238 water accumulatively produces 0.2–4.5 μM $\bullet\text{OH}$ (Minella et al., 2015); the oxidation of pyrite
239 can produce 7.5–135 μM $\bullet\text{OH}$ within 7 hours (Zhang & Yuan, 2017); and the oxidation of
240 river sediments can accumulatively produce 57–1479 $\mu\text{mol kg}^{-1}$ $\bullet\text{OH}$ within 48 hours (Liao et
241 al., 2019). Thus, the cumulative productions of $\bullet\text{OH}$ in this study are broadly similar to those
242 reported earlier from various environmental processes.

243 4.2 Stoichiometric production of $\bullet\text{OH}$ from superoxide and DOM-Fe(III)

244 In this study, the production of $\bullet\text{OH}$ is orders of magnitude larger in the presence than
245 the absence of introduced KO_2 , therefore, $\text{O}_2\bullet^-$ is responsible for the extensive production of
246 $\bullet\text{OH}$. The reaction pathway from $\text{O}_2\bullet^-$ to $\bullet\text{OH}$ is beyond the scope of the present study, because
247 we did not measure the intermediates such as DOM-Fe(II) or H_2O_2 . Our simple kinetic model,
248 however, successfully predicts the measured $R_f^{\bullet\text{OH}}(t_0)$ in the “ $\text{KO}_2 + \text{Fe}$ ” treatment and may
249 provide a mechanistic explanation for the initial $\bullet\text{OH}$ production rates (Text SI). According to
250 this simple model, the reaction pathway starts with the reduction of DOM-Fe(III) to DOM-

251 Fe(II) by $O_2^{\bullet-}$ (Eq.3, Text SI). Later, bimolecular disproportionation generates H_2O_2 (Eq.4).
252 At this stage, the reduction of O_2 by DOM-Fe(II) is the source of $O_2^{\bullet-}$ (Text SI). Finally, H_2O_2
253 reacts with DOM-Fe(II) (Eq.1, Text SI). The reactive oxygen species can maintain the redox
254 cycling of the iron catalyst and the production of $\bullet OH$ from the oxidant ($H_2O_2 = 2[O_2^{\bullet-} + H^+]$)
255 according to the stoichiometry of the Fenton reaction (Pignatello et al. 2006; Text SI).

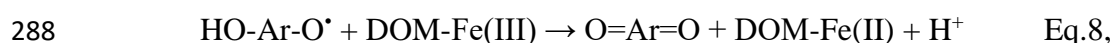
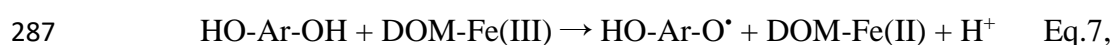
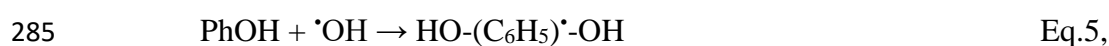


258 DOM facilitates the formation of $\bullet OH$ through the Fenton reaction in many ways
259 (Georgi et al., 2007). When DOM makes complexes with Fe(III) at $pH > 3.5$, it keeps Fe(III)
260 in soluble reactive form (Zhang & Zhou, 2019). At low pH (e.g., $pH = 5$ in this study), the
261 deprotonated carboxylic groups of DOM are favorable ligand for Fe(III) and the concentration
262 of a major competing ligand, hydroxyl ion (OH^-), is low (Bhattacharyya et al., 2019; Lee et al.,
263 2019; Neubauer et al., 2013; Zhang & Zhou, 2019). Mildly acidic conditions (like in the present
264 study) are favorable for the Fenton reaction, which breaks down humic substances most
265 efficiently at $pH 4-5$ rather than in more acidic or basic solutions (Wu et al., 2010).
266 Additionally, H_2O_2 reacts faster with DOM-Fe(II) than with inorganic Fe(II) (Voelker &
267 Sulzberger 1996; Zhang & Zhou, 2019).

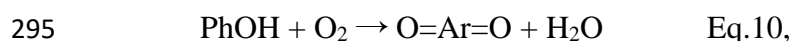
268 4.3 Autocatalysis of the Fenton reaction

269 In our study, the cumulative production of $\bullet OH$ is larger ($0.76-8 \bullet OH/O_2^{\bullet-}$) than
270 expected from the introduced $O_2^{\bullet-}$ according to the stoichiometry of the Fenton reaction (0.33
271 $\bullet OH/O_2^{\bullet-}$). The reactions between $\bullet OH$ and the phenolic moieties of DOM can explain the
272 autocatalysis of the Fenton reaction in this study (Voelker & Sulzberger, 1996, Chen &
273 Pignatello, 1997). Those reactions generate hydroquinone-like DOM and $O_2^{\bullet-}$ (Voelker &
274 Sulzberger, 1996, Chen & Pignatello, 1997, Duesterberg & Waite, 2007). The reactions

275 between $\bullet\text{OH}$ and phenols have been examined earlier with model compounds (phenol and
 276 hydroxybenzoic acid) that mimic the aromatic moieties of DOM (Chen & Pignatello, 1997;
 277 Duesterberg & Waite, 2007). Firstly, an addition of $\bullet\text{OH}$ to phenol (PhOH) generates a
 278 dihydroxycyclohexadienyl radical ($\text{HO}-(\text{C}_6\text{H}_5)\bullet\text{-OH}$, Eq.5), which transforms into
 279 hydroquinone (HO-Ar-OH) in a reaction that consumes O_2 and generates $\text{O}_2^{\bullet-}$ (Eq.6, Chen &
 280 Pignatello, 1997; Voelker & Sulzberger, 1996). Secondly, the transformation of hydroquinone
 281 to semiquinone radical ($\text{HO-Ar-O}\bullet$) reduces DOM-Fe(III) to DOM-Fe(II) (Eq.7, Chen &
 282 Pignatello, 1997; Duesterberg & Waite, 2007). Finally, a semiquinone radical reduces another
 283 DOM-Fe(III) when undergoing oxidation to quinone (O=Ar=O) (Eq.8, Chen & Pignatello,
 284 1997; Duesterberg & Waite, 2007).



290 The four consecutive reactions (Eq.5-8) described above produce three reducing
 291 equivalents ($\text{O}_2^{\bullet-}$ and/or DOM-Fe(II)) that re-generate the Fenton reactants and thus the
 292 production of $\bullet\text{OH}$ gets autocatalyzed through the Fenton reaction and DOM oxidation. Note
 293 that the net reaction of this process (from Eq.1 to Eq.9, with the exception of Eq.2) is the
 294 oxidation of phenol to quinone (Eq.10).



296 This autocatalysis can continue as long as water contains O_2 and DOM contains
 297 aromatic moieties that $\bullet\text{OH}$ can transform into hydroquinones. In this study, the headspace of
 298 air serves as a source of dissolved O_2 to our solutions like the atmosphere is a source of O_2 to

299 surface waters. The high (45–67%) aromaticity of DOM used in this study (Vogt et al., 2004)
300 provides a large reservoir of aromatic moieties that $\bullet\text{OH}$ can transform into hydroquinones.
301 Because highly aromatic humic substances and Fe are abundant in soils and freshwaters, the
302 potential for the autocatalyzed Fenton reaction is high in these environments.

303 4.4 Fenton reaction without introduced $\text{O}_2^{\bullet-}$

304 Our experiments show that even without introduction of $\text{O}_2^{\bullet-}$, DOM-Fe can produce
305 hydroxyl radicals at low amounts that are similar to $< 0.5 \mu\text{M}$ $\bullet\text{OH}$ produced during aeration
306 of Arctic surface waters (Page et al., 2012; Trusiak et al., 2018). Since Lake Valkea-Kotinen has
307 typically anoxic hypolimnion in late summer and it is surrounded by peaty soils, the DOM
308 extract used in the present study may contain Fe or quinone-like moieties in a reduced state.
309 The reduced hydroquinone-like moieties or reduced metals (e.g., Fe(II)) associated to DOM
310 can reduce O_2 to $\text{O}_2^{\bullet-}$ and initiate the sequence of reactions leading to the Fenton reaction (Garg
311 et al., 2018; Page et al., 2013, 2014). In this study, the external supply of DOM-Fe(III) doubled
312 the $\bullet\text{OH}$ production compared to DOM extract alone with low content of Fe and further
313 emphasizes the Fenton reaction as a source of $\bullet\text{OH}$. Although an abiotic dark formation of $\bullet\text{OH}$
314 is low in oxic surface waters without external source of $\text{O}_2^{\bullet-}$ (Trusiak et al., 2018; this study),
315 an episodic mixing of reduced DOM or redox sensitive metals to an oxic environment can
316 promote an extensive production of $\bullet\text{OH}$ (Minella et al., 2015; Page et al., 2012, 2013; Trusiak
317 et al., 2018).

318 4.5 Effects of $\text{O}_2^{\bullet-}$ and Fe on the absorption spectra of CDOM

319 In this study, the introduction of external $\text{O}_2^{\bullet-}$ eventually led to a CDOM break down
320 and increased the value of $S_{275-295}$ (Figure 1). These changes in CDOM are related to the
321 produced amount of $\bullet\text{OH}$ radicals and indicate that $\bullet\text{OH}$ rather than $\text{O}_2^{\bullet-}$ breaks down DOM
322 (Goldstone et al., 2002; Pignatello et al., 2006; Rush & Bielski, 2005; Waggoner et al., 2017;

323 Wu et al., 2010; this study). The changes in CDOM found in this study indicate a breakdown
324 of DOM into smaller less aromatic molecules (Helms et al., 2008) as found earlier in the
325 reactions between DOM and $\bullet\text{OH}$ (Goldstone et al., 2002; Pignatello et al., 2006).

326 4.6 Effects of $\text{O}_2^{\bullet-}$ and Fe on the fluorescence spectra of CDOM

327 In our study, the introduction of KO_2 without external supply of Fe(III) increases the
328 fluorescence of humic-like components (Figure 3), which agrees with the involvement of
329 hydroquinones in the autocatalysis of the Fenton reaction (Chen & Pignatello, 1997;
330 Duesterberg & Waite, 2007). The hydroxylation of aromatic moieties into hydroquinones by
331 $\bullet\text{OH}$ can explain the increase in fluorescence and no change in absorption in the first 26 h
332 (Figure 1a and 3), because hydroquinone-moieties have high fluorescence and absorption
333 (Cory et al., 2005). Additionally, the breakdown of DOM by $\bullet\text{OH}$ decreases the molecular size
334 of DOM and increases the spectral slope coefficient (Figure 1b), which are both related to an
335 increase in the quantum yield of fluorescence (Boyle et al., 2009; Senesi, 1990). The
336 complexation of Fe quenches fluorescence of DOM (Cabaniss, 1992; Du et al., 2018; Poulin
337 et al., 2014; Pullin et al., 2007; Figure 3), because Fe promotes internal conversion and
338 intersystem crossing of the first excited singlet state as well as a ligand to metal charge transfer,
339 i.e., processes that compete with fluorescence (Senesi, 1990). The reduction in fluorescence in
340 the “Fe + KO_2 ” treatment (Figure 3) is, instead, attributed to the breakdown of DOM by the
341 extensive amount of $\bullet\text{OH}$, suggesting that there is an optimum in fluorescence emission as a
342 function of DOM molecular weight or aromaticity.

343

344 **5 Conclusions**

345 This study shows that $\text{O}_2^{\bullet-}$ can induce the production of $\bullet\text{OH}$ in the presence of complexes
346 between Fe and humic DOM. The production of $\bullet\text{OH}$ can exceed the stoichiometry of Fenton
347 reaction by 2–24 folds. The autocatalysis of Fenton reaction observed in the present study

348 emphasizes the role of $O_2^{\bullet-}$ as an efficient transformer of organic matter. As numerous
349 processes (photochemistry, abiotic dark oxidation, and biology) can produce $O_2^{\bullet-}$, superoxide-
350 driven Fenton reactions likely transform natural organic matter and contaminants in diverse
351 terrestrial and freshwater environments.

352

353 **Author Contributions**

354 Y.X., L.C., and A.V.V. all contributed to the preparation, writing, and editing the manuscript.
355 Y.X. and M.-T.N. contributed to the sample collection and measurements. All authors reviewed
356 the manuscript.

357

358 **Declaration of competing interest**

359 The authors declare no competing financial interest.

360

361 **Acknowledgements**

362 This study was financially supported by the Academy of Finland Grant (No. 295709) and
363 Taishan Scholar Foundation of Shandong Province (No. tsqn201909126). The stay of L.C. in
364 Jyväskylä was financially supported by the Erasmus+ Traineeship programme. L.C.
365 acknowledges Compagnia di San Paolo (Torino, Italy) for financially supporting his Ph.D.
366 fellowship.

367

368 **Appendix A. Supplementary data**

369 Supplementary data to this article can be found online at ***.

370

371 **References**

372 Aarnos, H., Gélinas, Y., Kasurinen, V., Gu, Y., Puupponen, V.-M., & Vähätalo, A. V. (2018).

373 Photochemical Mineralization of Terrigenous DOC to Dissolved Inorganic Carbon in
374 Ocean. *Global Biogeochemical Cycles*, 32(2), 250–266.
375 <https://doi.org/10.1002/2017GB005698>

376 Aeschbacher, M., Schwarzenbach, R. P., & Sander, M. (2010). Novel electrochemical
377 approach to quantify the redox state of humic substances: Advantages and applications.
378 *Environmental Science & Technology*, 44(1), 87–93.

379 Arnosti, C. (2004). Speed bumps and barricades in the carbon cycle: Substrate structural
380 effects on carbon cycling. *Marine Chemistry*, 92(1-4 SPEC. ISS.), 263–273.
381 <https://doi.org/10.1016/j.marchem.2004.06.030>

382 Bhattacharyya, A., Schmidt, M. P., Stavitski, E., Azimzadeh, B., & Martínez, C. E. (2019).
383 Ligands representing important functional groups of natural organic matter facilitate Fe
384 redox transformations and resulting binding environments. *Geochimica et*
385 *Cosmochimica Acta*, 251, 157–175. <https://doi.org/10.1016/J.GCA.2019.02.027>

386 Boyle, E. S., Guerriero, N., Thiallet, A., Vecchio, R. Del, & Blough, N. V. (2009). Optical
387 Properties of Humic Substances and CDOM: Relation to Structure. *Environmental*
388 *Science & Technology*, 43(7), 2262–2268. <https://doi.org/10.1021/es803264g>

389 Burgos Castillo, R. C., Fontmorin, J. M., Tang Walter, Z., Xochitl, D. B., & Mika, S. (2018).
390 Towards reliable quantification of hydroxyl radicals in the Fenton reaction using
391 chemical probes. *RSC Advances*, 8(10), 5321–5330. <https://doi.org/10.1039/c7ra13209c>

392 Cabaniss, S. E. (1992). Synchronous fluorescence-spectra of metal-fulvic acid complexes.
393 *Environ. Sci. Technol.*, 26(6), 1133–1139.

394 Chen, R., & Pignatello, J. J. (1997). Role of quinone intermediates as electron shuttles in
395 Fenton and photoassisted Fenton oxidations of aromatic compounds. *Environmental*
396 *Science & Technology*, 31, 2399–2406. <https://doi.org/10.1021/ES9610646>

397 Cooper, W. J., & Zika, R. G. (1983). Photochemical formation of hydrogen peroxide in

398 surface and ground waters exposed to sunlight. *Science*, 220(4598), 711–712.
399 <https://doi.org/10.1126/science.220.4598.711>

400 Cory, R. M., McKnight, D. M., And, R. M. C., & McKnight, D. M. (2005). Fluorescence
401 spectroscopy reveals ubiquitous presence of oxidized and reduced quinones in dissolved
402 organic matter. *Environmental Science & Technology*, 39(21), 8142–8149.
403 <https://doi.org/10.1021/ES0506962>

404 Diaz, J. M., Hansel, C. M., Voelker, B. M., Mendes, C. M., Andeer, P. F., & Zhang, T.
405 (2013). Widespread production of extracellular superoxide by heterotrophic bacteria.
406 *Science*, 340(6137), 1223–1226. <https://doi.org/10.1126/science.1237331>

407 Diaz, Julia M., & Plummer, S. (2018). Production of extracellular reactive oxygen species by
408 phytoplankton: past and future directions. *Journal of Plankton Research*, 40, 655–666.
409 <https://doi.org/10.1093/plankt/fby039>

410 Dittmar, T., Koch, B., Hertkorn, N., & Kattner, G. (2008). A simple and efficient method for
411 the solid-phase extraction of dissolved organic matter (SPE-DOM) from seawater.
412 *Limnology and Oceanography: Methods*, 6(6), 230–235.
413 <https://doi.org/10.4319/lom.2008.6.230>

414 Du, Y., Ramirez, C. E., & Jaffé, R. (2018). Fractionation of dissolved organic matter by co-
415 precipitation with iron: Effects of composition. *Environmental Processes*, 5(1), 5–21.
416 <https://doi.org/10.1007/s40710-017-0281-4>

417 Duesterberg, C. K., & Waite, T. D. (2007). Kinetic modeling of the oxidation of p -
418 hydroxybenzoic acid by Fenton’s reagent: Implications of the role of quinones in the
419 Redox cycling of iron. *Environmental Science & Technology*, 41(11), 4103–4110.
420 <https://doi.org/10.1021/es0628699>

421 Einola, E., Rantakari, M., Kankaala, P., Kortelainen, P., Ojala, A., Pajunen, H., et al. (2011).
422 Carbon pools and fluxes in a chain of five boreal lakes: A dry and wet year comparison.

423 *Journal of Geophysical Research: Biogeosciences*, 116(3).
424 <https://doi.org/10.1029/2010JG001636>

425 Fujii, M., & Otani, E. (2017). Photochemical generation and decay kinetics of superoxide and
426 hydrogen peroxide in the presence of standard humic and fulvic acids. *Water Research*,
427 123, 642–654. <https://doi.org/10.1016/j.watres.2017.07.015>

428 Fujii, M., Imaoka, A., Yoshimura, C., & Waite, T. D. (2014). Effects of molecular
429 composition of natural organic matter on ferric iron complexation at circumneutral pH.
430 *Environmental Science and Technology*, 48(8), 4414–4424.
431 <https://doi.org/10.1021/es405496b>

432 Gao, H., & Zepp, R. G. (1998). Factors influencing photoreactions of dissolved organic
433 matter in a coastal river of the southeastern United States. *Environmental Science*
434 *& Technology*, 32, 2940–2946. Retrieved from <https://pubs.acs.org/sharingguidelines>

435 Garg, S., Rose, A. L., & Waite, T. D. (2011). Photochemical production of superoxide and
436 hydrogen peroxide from natural organic matter. *Geochimica et Cosmochimica Acta*,
437 75(15), 4310–4320. <https://doi.org/10.1016/j.gca.2011.05.014>

438 Garg, S., Jiang, C., & Waite, T. D. (2018). Impact of pH on iron redox transformations in
439 simulated freshwaters containing natural organic matter. *Environmental Science and*
440 *Technology*, 52(22), 13184–13194. research-article.
441 <https://doi.org/10.1021/acs.est.8b03855>

442 Georgi, A., Schierz, A., Trommler, U., Horwitz, C. P., Collins, T. J., & Kopinke, F. D.
443 (2007). Humic acid modified Fenton reagent for enhancement of the working pH range.
444 *Applied Catalysis B: Environmental*, 72(1–2), 26–36.
445 <https://doi.org/10.1016/j.apcatb.2006.10.009>

446 Gil-Lozano, C., Davila, A. F., Losa-Adams, E., Fairén, A. G., & Gago-Duport, L. (2017).
447 Quantifying Fenton reaction pathways driven by self-generated H₂O₂ on pyrite

448 surfaces. *Scientific Reports*, 7. <https://doi.org/10.1038/srep43703>

449 Goldstone, J. V., Pullin, M. J., Bertilsson, S., Voelker, B. M., & Hole, W. (2002). Reactions
450 of hydroxyl radical with humic substances : Bleaching , mineralization , and production
451 of bioavailable carbon substrates, *36*(3), 364–372. <https://doi.org/10.1021/ES0109646>

452 Goldstone, Jared V., & Voelker, B. M. (2000). Chemistry of superoxide radical in seawater:
453 CDOM associated sink of superoxide in coastal waters. *Environmental Science and*
454 *Technology*, *34*(6), 1043–1048. <https://doi.org/10.1021/es9905445>

455 Hayyan, M., Hashim, M. A., & AlNashef, I. M. (2016). Superoxide Ion: Generation and
456 Chemical Implications. *Chemical Reviews*, *116*(5), 3029–3085.
457 <https://doi.org/10.1021/acs.chemrev.5b00407>

458 Helms, J. R., Stubbins, A., Ritchie, J. D., Minor, E. C., Kieber, D. J., & Mopper, K. (2008).
459 Absorption spectral slopes and slope ratios as indicators of molecular weight, source,
460 and photobleaching of chromophoric dissolved organic matter. *Limnology and*
461 *Oceanography*, *53*(3), 955–969. <https://doi.org/10.4319/lo.2008.53.3.0955>

462 Hongve, D., Riise, G., & Kristiansen, J. F. (2004). Increased colour and organic acid
463 concentrations in Norwegian forest lakes and drinking water - A result of increased
464 precipitation? *Aquatic Sciences*, *66*(2), 231–238. [https://doi.org/10.1007/s00027-004-](https://doi.org/10.1007/s00027-004-0708-7)
465 [0708-7](https://doi.org/10.1007/s00027-004-0708-7)

466 Imlay, J. A. (2004). Pathways of Oxidative Damage. *Annual Review of Microbiology*, *57*(1),
467 395–418. <https://doi.org/10.1146/annurev.micro.57.030502.090938>

468 Karlsson, T., & Persson, P. (2012). Complexes with aquatic organic matter suppress
469 hydrolysis and precipitation of Fe(III). *Chemical Geology*, *322–323*, 19–27.
470 <https://doi.org/10.1016/j.chemgeo.2012.06.003>

471 Koehler, B., Landelius, T., Weyhenmeyer, G. A., Machida, N., & Tranvik, L. J. (2014).
472 Sunlight-induced carbon dioxide emissions from inland waters. *Global Biogeochemical*

473 *Cycles*, 28(7), 696–711. <https://doi.org/10.1002/2014GB004850>

474 Kothawala, D., Kellerman, A., Catalan, N., & Tranvik, L. (2016). Controls on the dynamics
475 of dissolved organic matter in boreal lakes. *Geophysical Research Abstracts EGU*
476 *General Assembly*, 18(April), 13894. [https://doi.org/10.1097/00010694-200004000-](https://doi.org/10.1097/00010694-200004000-00001)
477 00001

478 Lee, S., Roh, Y., & Koh, D.-C. (2019). Oxidation and reduction of redox-sensitive elements
479 in the presence of humic substances in subsurface environments: A review.
480 *Chemosphere*, 220, 86–97. <https://doi.org/10.1016/j.chemosphere.2018.11.143>

481 Liao, P., Yu, K., Lu, Y., Wang, P., Liang, Y., & Shi, Z. (2019). Extensive dark production of
482 hydroxyl radicals from oxygenation of polluted river sediments. *Chemical Engineering*
483 *Journal*, 368, 700–709. <https://doi.org/10.1016/j.cej.2019.03.018>

484 Louit, G., Foley, S., Cabillic, J., Coffigny, H., Taran, F., Valleix, A., et al. (2005). The
485 reaction of coumarin with the OH radical revisited: Hydroxylation product analysis
486 determined by fluorescence and chromatography. *Radiation Physics and Chemistry*,
487 72(2–3), 119–124. <https://doi.org/10.1016/j.radphyschem.2004.09.007>

488 Ma, J., Del Vecchio, R., Golanoski, K. S., Boyle, E. S., & Blough, N. V. (2010). Optical
489 properties of humic substances and CDOM: Effects of borohydride reduction.
490 *Environmental Science & Technology*, 44(14), 5395–5402.
491 <https://doi.org/10.1021/es100880q>

492 Micinski, E., Ball, L. A., & Zafiriou, O. C. (1993). Photochemical oxygen activation:
493 Superoxide radical detection and production rates in the eastern Caribbean. *Journal of*
494 *Geophysical Research: Oceans*, 98(C2), 2299–2306.
495 [https://doi.org/10.1029/92JC02766@10.1002/\(ISSN\)2169-9291.PECW1](https://doi.org/10.1029/92JC02766@10.1002/(ISSN)2169-9291.PECW1)

496 Minella, M., De Laurentiis, E., Maurino, V., Minero, C., & Vione, D. (2015). Dark
497 production of hydroxyl radicals by aeration of anoxic lake water. *Science of the Total*

498 *Environment*, 527–528, 322–327. <https://doi.org/10.1016/j.scitotenv.2015.04.123>

499 Mostovaya, A., Hawkes, J. A., Dittmar, T., & Tranvik, L. J. (2017). Molecular determinants
500 of dissolved organic matter reactivity in lake water. *Frontiers in Earth Science*, 5.
501 <https://doi.org/10.3389/feart.2017.00106>

502 Murphy, K. R., Stedmon, C. A., Graeber, D., & Bro, R. (2013). Fluorescence spectroscopy
503 and multi-way techniques. PARAFAC. *Analytical Methods*, 5(23), 6557.
504 <https://doi.org/10.1039/c3ay41160e>

505 Neubauer, E., Köhler, S. J., von der Kammer, F., Laudon, H., Hofmann, T., Neubauer, E., et
506 al. (2013). Effect of pH and stream order on iron and arsenic speciation in boreal
507 catchments. *Environmental Science & Technology*, 47(13), 1–14.
508 <https://doi.org/10.1021/es401193j>

509 Page, S. E., Sander, M., Arnold, W. A., & McNeill, K. (2012). Hydroxyl radical formation
510 upon oxidation of reduced humic acids by oxygen in the dark. *Environmental Science
511 and Technology*, 46(3), 1590–1597. <https://doi.org/10.1021/es203836f>

512 Page, S. E., Kling, G. W., Sander, M., Harrold, K. H., Logan, J. R., McNeill, K., & Cory, R.
513 M. (2013). Dark formation of hydroxyl radical in arctic soil and surface waters.
514 *Environmental Science and Technology*, 47(22), 12860–12867.
515 <https://doi.org/10.1021/es4033265>

516 Page, S. E., Logan, J. R., Cory, R. M., & McNeill, K. (2014). Evidence for dissolved organic
517 matter as the primary source and sink of photochemically produced hydroxyl radical in
518 arctic surface waters. *Environmental Sciences: Processes and Impacts*, 16(4), 807–822.
519 <https://doi.org/10.1039/c3em00596h>

520 Piccolo, A. (1996). *Humic substances in terrestrial ecosystems*. Amsterdam.

521 Pignatello, J. J., Oliveros, E., & MacKay, A. (2006). Advanced oxidation processes for
522 organic contaminant destruction based on the fenton reaction and related chemistry.

523 *Critical Reviews in Environmental Science and Technology*, 36(1), 1–84.
524 <https://doi.org/10.1080/10643380500326564>

525 Poulin, B. A., Ryan, J. N., & Aiken, G. R. (2014). The effects of iron on optical properties of
526 dissolved organic matter. *Environmental Science & Technology*, 48(17), 10098–10106.
527 <https://doi.org/10.1021/es502670r>

528 Pullin, M. J., Anthony, C., & Maurice, P. A. (2007). Effects of iron on the molecular weight
529 distribution, light absorption, and fluorescence properties of natural organic matter.
530 *Environmental Engineering Science*, 24(8), 987–997.
531 <https://doi.org/10.1089/ees.2006.0040>

532 Rose, A. L., & Waite, T. D. (2005). Reduction of organically complexed ferric iron by
533 superoxide in a simulated natural water. *Environmental Science & Technology*,
534 39(February), 2645–2650. <https://doi.org/10.1021/es048765k>

535 Rush, J. D., & Bielski, B. H. J. (2005). Pulse radiolytic studies of the reaction of
536 perhydroxyl/superoxide O₂⁻ with iron(II)/iron(III) ions. The reactivity of HO₂/O₂⁻ with
537 ferric ions and its implication on the occurrence of the Haber-Weiss reaction. *The*
538 *Journal of Physical Chemistry*, 89(23), 5062–5066. <https://doi.org/10.1021/j100269a035>

539 Senesi, N. (1990). Molecular and quantitative aspects of the chemistry of fulvic acid and its
540 interactions with metal ions and organic chemicals. *Analytica Chimica Acta*, 232, 77–
541 106. [https://doi.org/10.1016/S0003-2670\(00\)81226-X](https://doi.org/10.1016/S0003-2670(00)81226-X)

542 Southworth, B. A., & Voelker, B. M. (2003). Hydroxyl radical production via the photo-
543 Fenton reaction in the presence of fulvic acid. *Environmental Science & Technology*,
544 37(6), 1130–1136. <https://doi.org/10.1021/es020757l>

545 Tranvik, L. J. (1988). Availability of dissolved organic carbon for planktonic bacteria in
546 oligotrophic lakes of differing humic content. *Microbial Ecology*, 16(3), 311–322.
547 <https://doi.org/10.1007/BF02011702>

548 Trusiak, A., Treibergs, L. A., Kling, G. W., & Cory, R. M. (2018). The role of iron and
549 reactive oxygen species in the production of CO₂ in arctic soil waters. *Geochimica et*
550 *Cosmochimica Acta*, 224, 80–95. <https://doi.org/10.1016/j.gca.2017.12.022>

551 Vähätalo, A. V., Salonen, K., Münster, U., Järvinen, M., & Wetzel, R. G. (2003).
552 Photochemical transformation of allochthonous organic matter provides bioavailable
553 nutrients in a humic lake. *Archiv Fur Hydrobiologie*, 156(3), 287–314.
554 <https://doi.org/10.1127/0003-9136/2003/0156-0287>

555 Voelker, B. M., & Sulzberger, B. (1996). Effects of fulvic acid on Fe(II) oxidation by
556 hydrogen peroxide. *Environmental Science and Technology*, 30(4), 1106–1114.
557 <https://doi.org/10.1021/es9502132>

558 Voelker, B. M., Morel, F. M. M., & Sulzberger, B. (1997). Iron redox cycling in surface
559 waters: Effects of humic substances and light. *Environmental Science and Technology*,
560 31(4), 1004–1011. <https://doi.org/10.1021/es9604018>

561 Vogt, R. D., Akkanen, J., Andersen, D. O., Brüggemann, R., Chatterjee, B., Gjessing, E., et
562 al. (2004). Key site variables governing the functional characteristics of Dissolved
563 Natural Organic Matter (DNOM) in Nordic forested catchments. *Aquatic Sciences -*
564 *Research Across Boundaries*, 66(2), 195–210. [https://doi.org/10.1007/s00027-004-0710-](https://doi.org/10.1007/s00027-004-0710-0)
565 0

566 Waggoner, D. C., Wozniak, A. S., Cory, R. M., & Hatcher, P. G. (2017). The role of reactive
567 oxygen species in the degradation of lignin derived dissolved organic matter.
568 *Geochimica et Cosmochimica Acta*, 208, 171–184.
569 <https://doi.org/10.1016/j.gca.2017.03.036>

570 Wu, Y., Zhou, S., Qin, F., Peng, H., Lai, Y., & Lin, Y. (2010). Removal of humic substances
571 from landfill leachate by Fenton oxidation and coagulation. *Process Safety and*
572 *Environmental Protection*, 88(4), 276–284. <https://doi.org/10.1016/j.psep.2010.03.002>

573 Yuan, X., Davis, J. A., & Nico, P. S. (2016). Iron-mediated oxidation of
574 Methoxyhydroquinone under dark conditions: Kinetic and mechanistic insights.
575 *Environmental Science and Technology*, 50(4), 1731–1740.
576 <https://doi.org/10.1021/acs.est.5b03939>

577 Zhang, P., & Yuan, S. (2017). Production of hydroxyl radicals from abiotic oxidation of
578 pyrite by oxygen under circumneutral conditions in the presence of low-molecular-
579 weight organic acids. *Geochimica et Cosmochimica Acta*, 218, 153–166.
580 <https://doi.org/10.1016/j.gca.2017.08.032>

581 Zhang, T., Hansel, C. M., Voelker, B. M., & Lamborg, C. H. (2016). Extensive dark
582 biological production of reactive oxygen species in brackish and freshwater ponds.
583 *Environmental Science and Technology*, 50(6), 2983–2993.
584 <https://doi.org/10.1021/acs.est.5b03906>

585 Zhang, Yi, & Blough, N. V. (2016). Photoproduction of one-electron reducing intermediates
586 by chromophoric dissolved organic matter (CDOM): Relation to O₂⁻ and H₂O₂
587 photoproduction and CDOM photooxidation. *Environmental Science and Technology*,
588 50(20), 11008–11015. <https://doi.org/10.1021/acs.est.6b02919>

589 Zhang, Ying, & Zhou, M. (2019). A critical review of the application of chelating agents to
590 enable Fenton and Fenton-like reactions at high pH values. *Journal of Hazardous*
591 *Materials*, 362, 436–450. <https://doi.org/10.1016/j.jhazmat.2018.09.035>
592

593 **Tables**594 **Table 1.** Experimental design. The initial concentrations of DOM, complexed Fe, KO₂, and

595 coumarin in the treatments made in artificial lake water (Table S1).

Treatments	DOM (mg L ⁻¹)	Fe (μM)	KO ₂ (μM)	Coumarin (μM)
control	20	0.17 [*]	--	10
KO ₂ ^{***}	20	0.17 [*]	13	10
Fe	20	20 ^{**}	--	10
Fe + KO ₂ ^{***}	20	20 ^{**}	13	10

596 --, no addition of KO₂. ^{*} residual Fe in extracted DOM (8.5 nmol Fe/mg DOM), ^{**} introduced
597 as DOM-Fe complex. ^{***}In the treatments “KO₂” and “Fe + KO₂”, the introduction of 13 μM
598 KO₂ increased pH to 12.2, which was soon titrated with HCl back to the same pH 5 as in the
599 other treatments.

600

601 **Table 2.** Cumulative production of •OH radicals (μM) in the treatments.
602

Time Interval	control	Fe	KO ₂	Fe + KO ₂
0–10 h	0.09	0.11	1.32	16.3
0–168 h	0.23	0.57	9.88	103.5

603

604 **Figure captions**

605 **Figure 1.** Absorption coefficient of CDOM at 410 nm (a_{410}) and spectral slope coefficient (S_{275-}
606 $_{295}$) after 26 h and 168 h incubations in the three treatments and the control. Table 1 explains
607 the treatments. Stars indicate a significant difference between the treatments and the control, *
608 $P < 0.05$ and ** $P < 0.01$. Error bars show standard deviations of three replicated treatments.

609

610 **Figure 2.** Overlaid spectra of four components (PARAFAC model). The figure shows six
611 unique splits vs. the overall model. Dot lines indicate excitation spectra and solid lines indicate
612 emission spectra. The excitation and emission maxima of each components are shown in Table
613 S2. The loadings in the Y-axis indicate the normalized component intensity in the PARAFAC
614 modeling.

615

616 **Figure 3.** Fluorescent intensities at 168 h of four components obtained from EEM-PARAFAC
617 modeling (Figure 2). The fluorescence of component 4 was negligible in the “Fe+KO₂”
618 treatment. Stars indicate a significant difference between treatment and the control, * $P < 0.05$
619 and ** $P < 0.01$. Error bars show standard deviations of three replicated treatments.

620

621 **Figure 4.** Computed formation rate of •OH in the treatments at selected times (■). The blue
622 lines represent the fitting functions from which the cumulative production of •OH radicals were
623 calculated. The R² parameter shows the goodness of the fit. See SI for the fitting functions.
624 Note the orders of magnitude differences in the scales of Y-axes.

625